Morphological Transformation of PS-*b*-PEO Diblock Copolymer by Selectively Dispersed Colloidal CdS Quantum Dots

Siao-Wei Yeh and Kung-Hwa Wei*

Department of Materials Science and Engineering, National Chiao Tung University, Hsinchu, Taiwan 30049, ROC

Ya-Sen Sun, U-Ser Jeng, and Keng S. Liang

National Synchrotron Radiation Research Center, 101 Hsin-Ann Road, Science-Based Industrial Park, Hsinchu, Taiwan 30077, ROC

Received June 11, 2003
Revised Manuscript Received August 28, 2003

Block copolymers are versatile platform materials because they can self-assemble into various nanostructures with period thicknesses between 10 and 100 nm under the appropriate compositions and conditions, owing to microphase separation between incompatible blocks.[1−3] In recent years, a number of studies involving applications of nanostructured block copolymer as nanotemplate,[4−6] nanomasks for lithography,[7] and photonic crystal[8] have been reported. Specifically, the work on nanometer-scale surface pattern with long-range order created by crystallization of asymmetric PB-*b*-PEO by Reiter[4b,c] is an interesting one. In another case, sorting out different sizes of CdSe nanoparticles into PS-*b*-PMMA porous template with capillary force was carried out by Russell et al.[5a] Several groups also reported the use of block copolymer as nanotemplates to grow Co, Ag, and Au nanowires[5b−d] or to control the spatial locations of nanoparticles[6b,d] such as TiO_2 and Pd. Moreover, block copolymer lithography with large area nanoscale patterning by Register et al.[7a,b] has also been reported. These studies motivated us to investigate the interaction between the block copolymer and nanoparticles, particularly on the effect of nanoparticles in the morphology of block copolymers.

For semiconductor nanoparticles with sizes close to their Bohr exciton radius (typically between 1 and 10 nm), the size-dependent band gap results in tunable optical properties.[9,10] These semiconductor nanoparticles are termed quantum dots (QDs) because their tunable optical properties can be predicted by quantum mechanics. Nanoparticles that are not treated with a surfactant or bonded to polymer chains will, however, form large aggregates.

The use of nanostructured block copolymers as templates to selectively control the spatial location of semiconductor nanoparticles in one of the blocks may lead to several potential applications. For instance, periodic high refractive index contrast domains in phase-separated block copolymers can be used in photonic crystal applications. Nanoparticles with highly efficient luminescence can be combined with organic layers in light-emitting devices.[11] The incorporation of nanoparticles into block copolymers, however, would lead to more complicated block copolymer morphologies than their pristine state as predicted by Balazs' group,[12] which used a self-consistent-field theory and a density functional theory for describing the polymer and the nanoparticles, respectively, to predict the morphology and phase diagram. In this Communication, we report the selective distribution of CdS QDs in the PEO block of a diblock copolymer, PS-*b*-PEO, and the resultant morphological changes. Specifically, CdS QDs induce the PEO domains to change from hexagonally packed cylinders to body-centered-cubic or simple-cubic spheres, as shown in Scheme 1. To our knowledge, this is the first study concerning the morphological transformation of block copolymer by nanoparticles.

Scheme 1. Morphological Transformation of PS-*b*-PEO Diblock Copolymer by Selectively Dispersed Colloidal CdS QDs

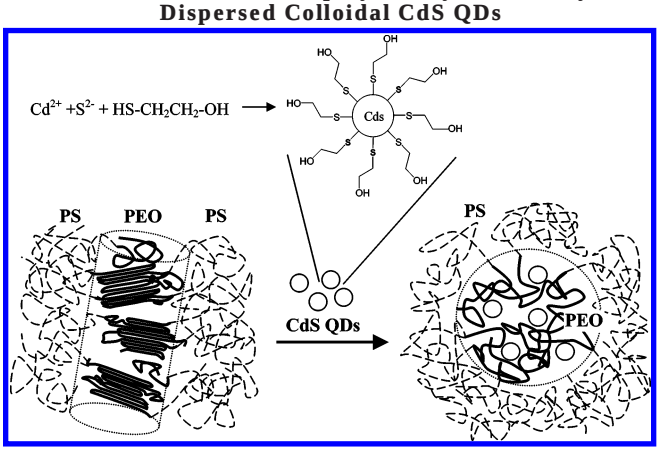

For the present study, an asymmetric polystyrene-*b*-poly(ethylene oxide) diblock copolymer (PS-*b*-PEO) with a molecular weight ratio of 125K/16.1K was purchased from Polymersource Inc. The volume fraction of PEO in this PS-*b*-PEO is 0.11, with a polydispersity of 1.04. CdS nanoparticles were synthesized with mercaptoethanol as the surfactant by reacting cadmium acetate dehydrate ($Cd(Ac)_2{\cdot}2H_2O$), sodium sulfide (Na_2S), and mercaptoethanol (HSC_2H_4OH) in methanol, following a modification of the kinetic trapping method.[10] After filtration, CdS QDs were collected and then dispersed in *N*,*N*-dimethylformamide (DMF). In our case, surfactant-modified CdS containing a chemically active hydroxyl surface, as shown in Scheme 1, became hydrophilic, and their basic properties are given in Table 1. In Table 1, the averaged size of CdS QDs is about 2.5 nm as determined from SAXS curves of CdS/PS-*b*-PEO in Figure 1 because in the higher Q region ($Q > 0.07$ Å^{-1}) where the scattering is dominated by form factor, the SAXS curves can be modeled using a sphere form factor of radius 2.5 nm. The sizes of CdS calculated from the onset absorption of the UV−vis spectrum typically represent the larger size in the size distribution curve of CdS in DMF.[6] Moreover, the CdS size obtained from the X-ray diffraction is the crystal size, which is the smallest and corresponds to the fact that we have polycrystal CdS. Subsequently, CdS/DMF was added to a previously prepared PS-*b*-PEO/DMF solution under stirring. This mixture was dried slowly under vacuum at 323 K and then maintained at 383 K for 24 h, after which the CdS/PS-*b*-PEO nanocomposite film was obtained. Preparation of pure PS-*b*-PEO films is similar to that of CdS/PS-*b*-PEO, except the lack of CdS. Thermal gravity analysis had been used to check the presence of the residual DMF solvent, and there was

* To whom correspondence should be addressed: Tel 886-35-731871; Fax 886-35-724727; e-mail khwei@cc.nctu.edu.tw.

10.1021/ma034800g CCC: $25.00
Published on Web 09/18/2003

Table 1. Characteristic Properties of CdS Nanoparticles

absorption onset (λ_o)[a]	particle size in DMF[b]	emission wavelength[c]	crystal size[d]	av particle size[e]
447 nm	3.37 nm	650 nm	1.33 nm	2.5 nm

[a] The onset absorption wavelength of CdS nanoparticles in DMF as obtained from UV−vis spectra. [b] The sizes of CdS nanoparticles in DMF were calculated with the onset absorption obtained by UV−vis spectra using the following equation:[6,9,10] $E_{g,os} - E_{g,ref} = \Delta E_g \approx (\hbar^2\pi^2/2R^2)(1/\mu) - (1.8e^2/\epsilon R)$. [c] The emission wavelength is determined from the photoluminescence. [d] Crystal sizes are calculated using the Debye−Scherrer equation. [e] The averaged size of CdS was obtained from SAXS curves of CdS/PS-*b*-PEO in Figure 1.

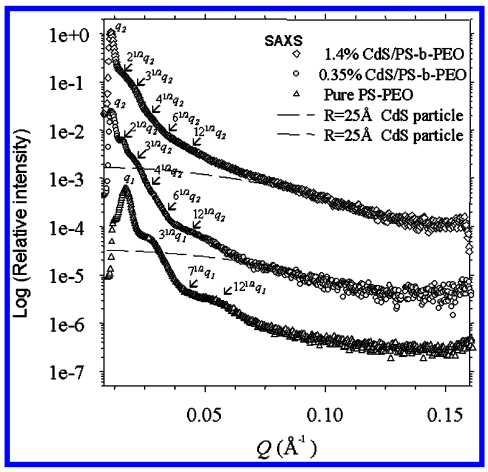

Figure 1. Synchrotron SAXS curves of PS-*b*-PEO and CdS/PS-*b*-PEO.

no residual DMF present in these block copolymer nanocomposites.

Small-angle X-ray scattering experiments were performed on wiggler beamline BL-17B1 at the National Synchrotron Radiation Research Center, Taiwan. Wide-angle X-ray diffraction on samples was collected by using a conventional rotating anode source. For transmission electron microscopy (TEM) and atomic force microscopy (AFM), the thin specimens were microtomed with Leica Ultracut Uct. TEM images were obtained with Hitachi H-600 transmission electron microscope. AFM measurements were performed in tapping mode with a Digital Nanoscope IIIa under ambient conditions. The glass transition temperatures (T_g) and melting point (T_m) were obtained from a Dupont DSC 2910 at a heating rate of 20 °C/min. Photoluminescence spectra (PL) were obtained with a Hitachi F4500 fluorescence spectrophotometer at room temperature.

Figure 1 shows one-dimensional small-angle X-ray scattering patterns (SAXS) of PS-*b*-PEO and CdS/PS-*b*-PEO nanocomposites by synchrotron radiation. For pure PS-*b*-PEO, four peaks appear at $Q = 0.016$, 0.027, 0.032, and 0.042 Å^{-1}, corresponding to a ratio of $1:3^{1/2}:4^{1/2}:7^{1/2}$. This ratio indicates typical scattering by hexagonally packed cylinders (HEX). The intercylinder distance (D) was determined to be 45.3 nm by eq 1.

$$D = ({}^4/_3)^{1/2} d_{100} \qquad (1)$$

where $d_{100} = 2\pi/Q_{100}$ and $Q_{100} = 0.16$ nm^{-1}. In the case of PS-*b*-PEO containing 0.35% CdS, the scattering peaks are located at $Q = 0.0114$, 0.0158, 0.0203, 0.0228, 0.0281, and 0.0399 Å^{-1}, which gives a ratio of $1: 2^{1/2}:3^{1/2}:4^{1/2}:6^{1/2}:12^{1/2}$. This ratio implies that the scattering is caused by either body-centered-cubic packed spheres (bcc) or simple-cubic spheres (sc). The intersphere distance is 67.5 nm, as determined from eq 2.

$$D = ({}^3/_2)^{1/2} d_{100} \qquad (2)$$

where $d_{110} = 2\pi/Q_{110}$ and $Q_{110} = 0.114$ nm^{-1}. SAXS results confirm that the nanostructured HEX structure of pure PS-*b*-PEO has been transformed to a bcc or sc morphology due to the presence of CdS QDs. The size of CdS QDs in the block copolymer is about 2.5 nm, as derived from the structure form of the SAXS curve.

Parts a and b of Figure 2 show the transmission electron microscopy (TEM) images of PS-*b*-PEO stained with OsO_4 and CdS/PS-*b*-PEO without staining, respectively. PEO domains appear in dark phase in Figure 2a, owing to selective staining, and display as short cylinders. In the case of CdS/PS-*b*-PEO, however, periodic dark spherical phases of CdS-included PEO appear, and no pure PEO domains without CdS QDs could be observed. The location of CdS in the PEO domain is revealed by energy dispersive spectrometry. Dark phases are caused by the higher electron density of cadmium relative to that of PS-*b*-PEO. The selective distribution of mercaptoethanol-modified CdS in the PEO domain is quite possibly due to dipole−dipole interactions between the hydroxyl groups of mercaptoethanol and the PEO block. The diameter of CdS-included PEO spheres is approximately 23 nm and the intersphere distance is about 60 nm, as estimated from their TEM images. To cover all PEO domains, there must be some distributions of CdS QDs in each PEO domain because the volume fraction of added CdS with respect to the PEO block is about 2.7%, which is not enough to cover each PEO domain fully. It is, however, not possible to detect them with the current techniques.

The results from TEM analysis are consistent with those by SAXS. Further evidence of the two different morphologies can be found in phase-contrast atomic force microscopy images (AFM) of PS-*b*-PEO and CdS/PS-*b*-PEO samples, as shown in parts c and d of Figure 2, respectively. A diamond knife used during the microtoming process causes the oblique lines in these figures. The difference in the images of pure PS-*b*-PEO by TEM and AFM (Figure 2a,c) could be explained by the fact that the dark PEO domains which appear as inclined short cylinders in bulk can be projected into cylindrical shapes in the transmission electron microscopy study, whereas the topology of the same microtomed slice would shows hairy spherical images by the tapping mode of AFM.

Figure 3a shows the thermal analysis results of PS-*b*-PEO and CdS/PS-*b*-PEO by differential scanning calorimetry. A crystal melting peak at 42.9 °C associated with the PEO domain and a glass transition temperature (T_g) at 99 °C attributed to the PS domain appear in the pure PS-*b*-PEO case. (The amorphous phase of PEO is rather small and undetectable.) In the presence of CdS, the crystal melting peak of PEO depressed and diminished to a small kink, with an apparent T_g of −56.6 °C. The PS domain, however, maintains a T_g of about 99 °C. The difference between the two cases can be explained by a loss of crystallinity in the PEO domain by the infiltration of CdS QDs into the PEO domain. Moreover, the wide-angle X-ray diffraction results shown in Figure 3b,c also support the corresponding crystal-to-amorphous change of the PEO domain. In the case of pure PS-*b*-PEO, two sharp peaks at 1.35 and 1.63 Å^{-1}

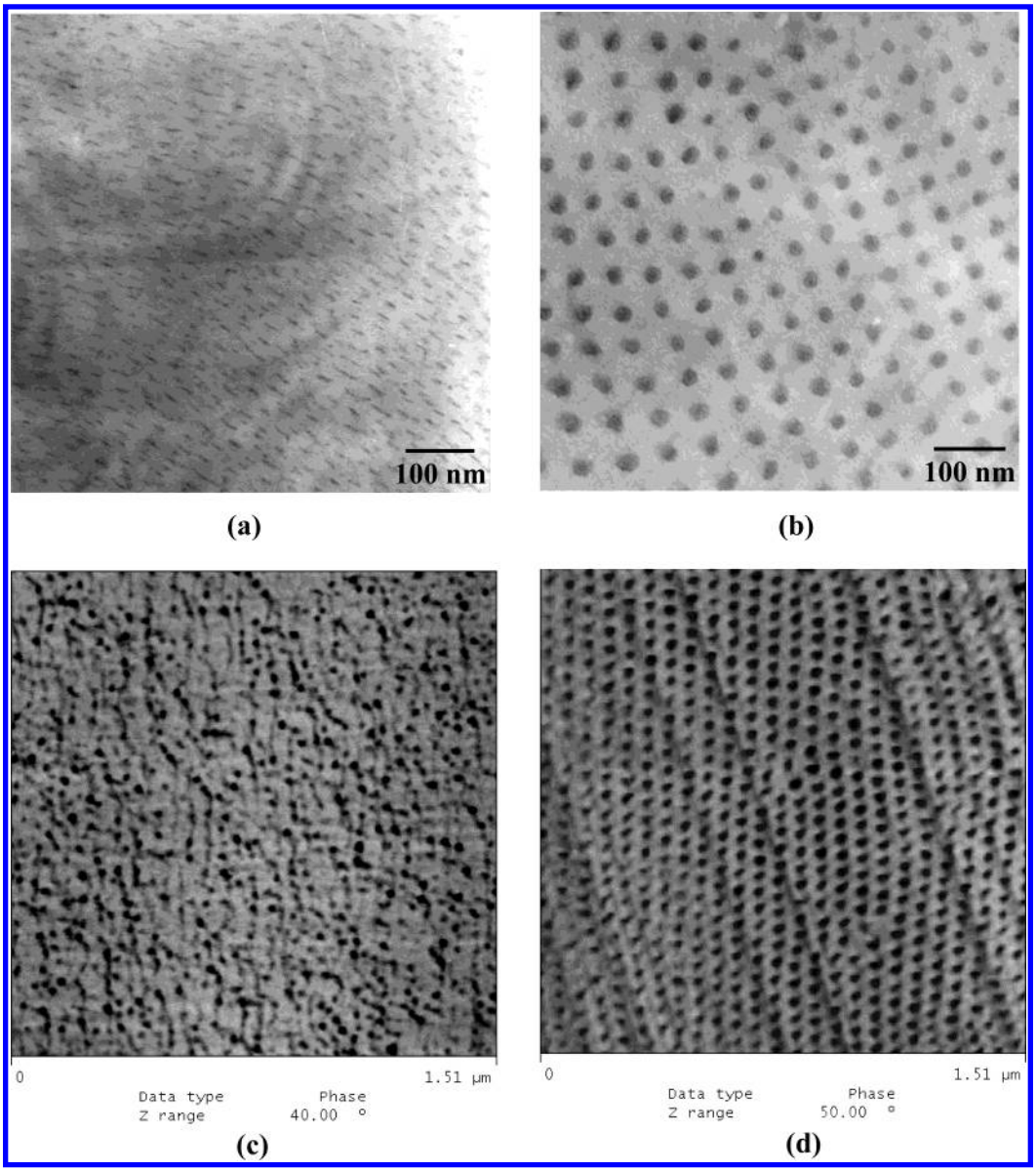

Figure 2. (a) TEM image of PS-*b*-PEO stained by OsO_4. The dark regions correspond to PEO phases stained with OsO_4. (b) TEM image of CdS/PS-*b*-PEO without staining. (c) AFM images of thin films microtomed from bulk PS-*b*-PEO and (d) AFM images of thin films microtomed from bulk CdS/PS-*b*-PEO.

represent the crystallinity peaks of the PEO domain after deconvolution, as shown in Figure 3b. Figure 3c shows amorphous X-ray diffraction curves when CdS is incorporated into the PEO domain, indicating the change from crystalline to amorphous PEO. This result is also consistent with those obtained by DSC. The possible scenario for this phenomenon is due to the relatively small size of CdS to the contour length of PEO block (2.5 nm vs 130 nm) and the dipole−dipole interaction between the angling hydroxy group of surface-attached mercaptoethanol on CdS and ethylene oxide in the PEO domain; CdS is tethering to the PEO chain and appears to destroy the crystallinity of the PEO domain, as shown in Scheme 1. This enables CdS-infiltrated PEO domains to be amorphous and to minimize their surface energy by forming either bcc or sc structures.

When only the volume fraction of the block copolymer PS-*b*-PEO is considered, it is true that in the equilibrium state the pure PS-*b*-PEO should be in the spherical region with body-centered-cubic packing due to strong segregation.[13] The morphology of asymmetric amorphous−crystalline block copolymers, however, depends on both the microphase separation of the two blocks and the crystallization kinetics of the crystallizable block as demonstrated in the work by de Jeu et al.[14] In their study, lamellar or hexagonally perforated lamellar structures of PS-*b*-PEO were obtained even though the volume fraction of PS-*b*-PEO indicates that it is typically within the morphological range of sphere or cylinders. In our study, the hexagonally packed cylindrical morphology of PS-*b*-PEO represents a compromise between the microphase separation involving PS and PEO blocks and the crystallization kinetics of the PEO block.[13,14] The cylindrical morphology of pure PS-*b*-PEO is in a metastable state due to the fast crystallization of the PEO block. The addition of CdS quantum dots into the diblock copolymer inhibits the crystallization of PEO block. The resultant morphology of CdS/PS-*b*-PEO sample, therefore, is determined largely by the microphase separation involving PS block and CdS/PEO block, (i.e., the crystallization effect no longer exists).

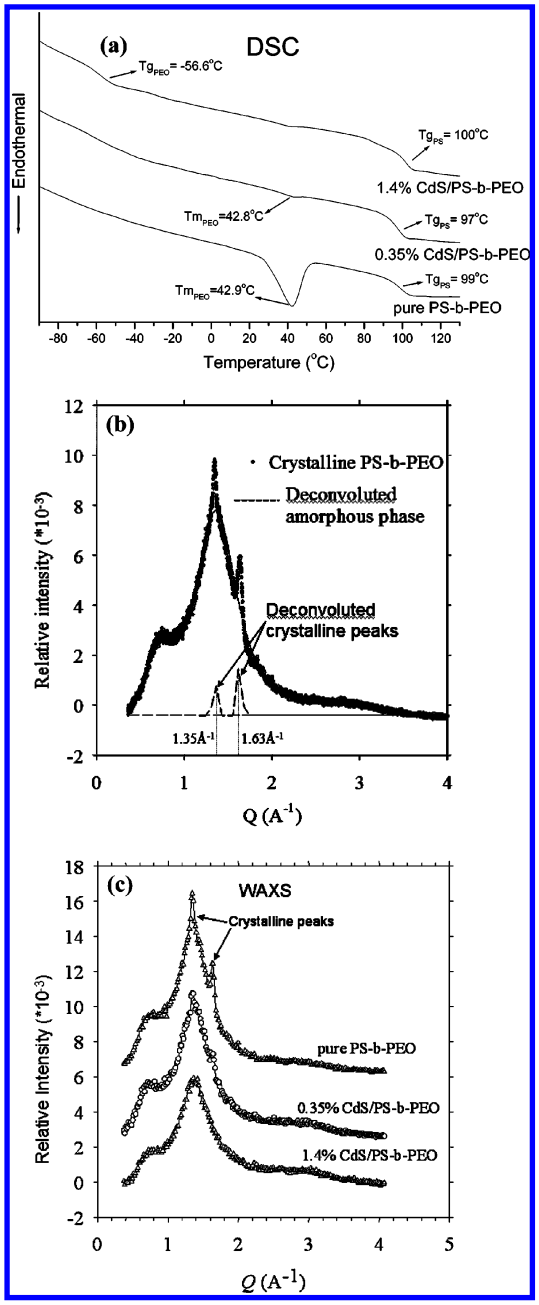

Figure 3. (a) DSC analysis of CdS/PS-*b*-PEO and PS-*b*-PEO. The samples were heated from −90 to 130 °C at 10 °C/min. (b) Deconvolution curves of the WAXS curve of crystallinity PS-*b*-PEO. (c) WAXS of PS-*b*-PEO and CdS/PS-*b*-PEO after crystallization at −20 °C for 18 h.

Theoretically, it is possible to observe the morphological transformation of pure PS-*b*-PEO, providing two requirements are satisfied—at high temperature (far above T_m of PEO and T_g of PS) and long time (diffusion rate of polymer melt is very small). In reality, this phenomenon may not happen for pure PS-*b*-PEO since the block copolymer might start to degrade if it were maintained at high temperature for too long.

Photoluminescence spectra of CdS QDs in DMF and the CdS/PS-*b*-PEO nanocomposite film are shown in Figure 4. CdS QDs in DMF emit red light with a maximum intensity located at 650 nm. The peak maximum of CdS in the PEO block of PS-*b*-PEO is red-shifted by 30 nm compared to CdS in DMF. The red shift in the luminescence of CdS QDs might be caused by aggregation or the different chemical environment.[10]

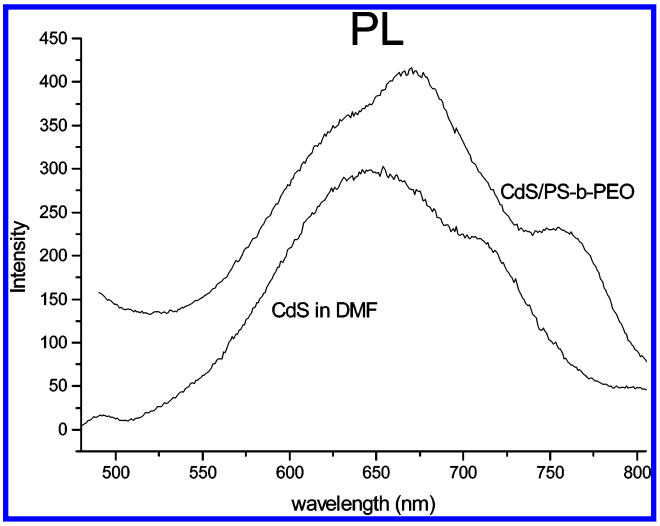

Figure 4. Photoluminescence of CdS and CdS/PS-*b*-PEO after excitation with 430 nm light.

In conclusion, semiconductor CdS QDs can be selectively dispersed in the PEO domain of PS-*b*-PEO block copolymer by using a surfactant. The CdS-infiltrated PEO domains are transformed from originally hexagonally packed cylindrical structures to bcc or sc structures because CdS inhibits the crystallization and minimizes the surface energy of CdS-infiltrated PEO phase. The photoluminescence of CdS is slightly affected by their incorporation in PS-*b*-PEO.

Acknowledgment. The authors acknowledge the National Science Council for funding this work through NSC 91-2120-M-009-001. Mr. Tsung-Lun Wu is appreciated for his help in experiments and discussions.

References and Notes

(1) (a) Bates, F. S.; Fredrickson, G. H. *Annu. Rev. Phys. Chem.* **1990**, *41*, 525. (b) Bates, F. S. *Science* **1991**, *251*, 898.

(2) (a) Zhu, L.; Stephen, Z. D.; Cheng; Huang, P.; Ge, Q.; Quirk, R. P.; Thomas, E. L.; Lotz, B.; Hsiao, B. S.; Yeh, F.; Liu, L. *Adv. Mater.* **2002**, *14*, 31. (b) Choi, S.; Lee, K. M.; Han, C. D.; Sota, N.; Hashimoto, T. *Macromolecules* **2003**, *36*, 793. (c) Buck, E.; Fuhrmann, J. *Macromolecules* **2001**, *34*, 2172.

(3) (a) Loo, Y. L.; Register, R. A.; Ryan, A. J. *Macromolecules* **2002**, *35*, 2365. (b) Loo, Y. L.; Register, R. A.; Ryan, A. J.; Dee, G. T. *Macromolecules* **2001**, *34*, 8968. (c) Rottele, A.; Thurn-Albrecht, T.; Sommer, J. U.; Reiter, G. *Macromolecules* **2003**, *36*, 1257.

(4) (a) Kim, D. H.; Lin, Z.; Kim, H. C.; Jeong, U.; Russell, T. P. *Adv. Mater.* **2003**, *15*, 811. (b) Reiter, G.; Castelein, G.; Sommer, J. U.; Rottele, A.; Thurn-Albrecht, T. *Phys. Rev. Lett.* **2001**, *87*, 226101. (c) Reiter, G.; Castelein, G.; Hoerner, P.; Riess, G.; Blumen, A.; Sommer, J. U. *Phys. Rev. Lett.* **1999**, *83*, 3844. (d) Boker, A.; Knoll, A.; Elbs, H.; Abetz, V.; Muller, A. H. E.; Krausch, G. *Macromolecules* **2002**, *35*, 1319.

(5) (a) Misner, M. J.; Skaff, H.; Emrick, T.; Russell, T. P. *Adv. Mater.* **2003**, *15*, 221. (b) Thurn-Aibrecht, T.; Schotter, J.; Castle, G. A.; Emley, N.; Shibauchi, T.; Krusin-Elbaum, L.; Guarini, K.; Black, C. T.; Touminen, M. T.; Russell, T. P. *Science* **2000**, *290*, 2126. (c) Lopes, W. A. *Phys. Rev. E* **2002**, *65*, 31606. (d) Lopes, W. A.; Jaeger, H. M. *Nature (London)* **2001**, *414*, 735.

(6) (a) Moffitt, M.; Vali, H.; Eisenberg, A. *Chem. Mater.* **1998**, *10*, 1021. (b) Weng, C. C.; Wei, K. H. *Chem. Mater.* **2003**, *15*, 2936. (c) Bockstaller, M. R.; Lapetnikov, Y.; Margel, S.; Thomas, E. L. *J. Am. Chem. Soc.* **2003**, *125*, 5276. (d) Ribbe, A. E.; Okumura, A.; Matsushige, K.; Hashimoto, T. *Macromolecules* **2001**, *34*, 8239.

(7) (a) Park, M.; Chaikin, P. M.; Register, R. A.; Adamson, D. H. *Appl. Phys. Lett.* **2001**, *79*, 257. (b) Park, M.; Harrison,

C.; Chaikin, P. M.; Register, R. A.; Adamson, D. H. *Science* **1997**, *276*, 1401. (c) Kim, H. C.; Jia, X.; Stafford, C. M.; Kim, D. H.; McCarthy, T. J.; Tuominen, M.; Hawker, C. J.; Russell, T. P. *Adv. Mater.* **2001**, *13*, 795. (d) Cheng, J. Y.; Ross, C. A.; Thomas, E. L.; Smith, H. I.; Vancso, G. J. *Appl. Phys. Lett.* **2002**, *81*, 3657.

(8) Urbas, A. M.; Maldovan, M.; DeRege, P.; Thomas, E. L. *Adv. Mater.* **2002**, *14*, 1850.

(9) (a) Zhang, J. Z. *Acc. Chem. Res.* **1997**, *30*, 423. (b) Brus, L. *J. Phys. Chem.* **1986**, *90*, 2555.

(10) (a) Veinot, J. G. C.; Ginzburg, M.; Pietro, W. J. *Chem. Mater.* **1997**, *9*, 2117. (b) Herron, N.; Wang, Y.; Eckert, H. *J. Am. Chem. Soc.* **1990**, *112*, 1322.

(11) (a) Gao, M. Y.; Richter, B.; Kirstein, S. *Adv. Mater.* **1997**, *9*, 802. (b) Gao, M. Y.; Richter, B.; Kirstein, S.; Mohwald, H. *J. Phys. Chem. B* **1998**, *102*, 4096.

(12) (a) Thompson, R. B.; Ginzburg, V. V.; Matsen, M. W.; Balazs, A. C. *Science* **2001**, *292*, 2469. (b) Thompson, R. B.; Ginzburg, V. V.; Matsen, M. W.; Balazs, A. C. *Macromolecules* **2002**, *35*, 1060. (c) Lee, J. Y.; Thompson, R. B.; Jasnow, D.; Balazs, A. C. *Macromolecules* **2002**, *35*, 4855.

(13) Hamley, I. W. *The Physics of the Block Copolymers*, Oxford University Press: New York, 1998.

(14) Li, L.; Serero, Y.; Koch, M. H. J.; de Jeu, W. H. *Macromolecules* **2003**, *36*, 529.

MA034800G